ACS Catalysis

Research Article

pubs.acs.org/acscatalysis

Unraveling the Role of Metal−Support Interactions in Heterogeneous Catalysis: Oxygenate Selectivity in Fischer−Tropsch Synthesis

Glen R. Jenness and J. R. Schmidt*

Department of Chemistry and Theoretical Chemistry Institute, University of Wisconsin−Madison, 1101 University Avenue, Madison, Wisconsin 53706, United States

Supporting Information

ABSTRACT: We examine the role of the metal−support interaction in modulating the activity and selectivity of oxide-supported metal nanoparticles, focusing specifically on the Fischer−Tropsch (FT) synthesis of ethanol (EtOH). Although it is well-known that oxide supports can play a noninnocent role in heterogeneous catalysis, a comprehensive and predictive picture of the role of such supports remains elusive. Using realistic computational models of supported nanoparticles, we decouple the electronic and geometric aspects of the metal−support interaction, and we show that the former can be largely understood in terms of charge transfer between support and nanoparticle. The resulting metal−support interactions induce significant changes in adsorbate binding energies, and thus significantly influence reaction thermodynamics and kinetics. For the specific case of FT, we show how our model can be used to understand the observed increase in EtOH selectivity when switching from silica to titania supports. More generally, we illustrate how these ideas can be used to crudely predict the influence of a support even in the absence of detailed calculations and provide a general framework for understanding the influence of various oxide supports on elementary association/dissociation reactions.

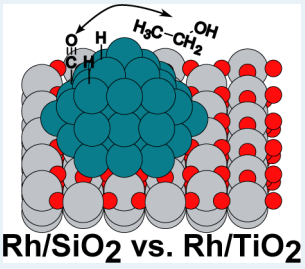

KEYWORDS: *heterogeneous catalysis, Fischer−Tropsch, syngas, rhodium, metal, support, oxide*

1. INTRODUCTION

Heterogeneous catalysts are ubiquitous in large-scale chemical production, with applications ranging from petrochemistry to fine chemistry and pharma.[1] Yet a comprehensive and predictive understanding of these catalytic processes is hindered by the complexity of industrially relevant catalysts under operating reactor conditions. While practical heterogeneous catalysts are typically composed of metal nanoparticles supported on metal oxide (often with added promoters), both computational and experimental surface science approaches often focus on "model" single-crystal materials, constituting the well-known "materials gap".[1,2] Although such model studies have yielded significant insight into catalytic mechanisms and activity, they frequently omit subtle (but crucial) aspects including structure sensitivity and the role of the metal−support interaction.

In particular, the influence of the support on catalytic activity and selectivity has long been recognized. The well-known strong metal−support interaction[3,4] (SMSI) describes the (often detrimental) reduced chemisorption following high temperature reduction (typically for nanoparticles on reducible oxide supports) due to a combination of encapsulation of the nanoparticle by the support and/or charge transfer between support and nanoparticle.[5−18] However, more recently a broader view of electronic metal−support interactions (EMSI) was outlined by Campbell,[5] encompassing both beneficial electronic (charge transfer,[5,6] ligand effects,[19−22] etc.) and geometric interactions (strain, relaxation, etc.) between the nanoparticle and support, as well as the possibility for reactions at special sites at the metal-oxide boundary.[23−27] This perspective opens the door to exploiting specific metal−support interactions to optimize catalytic transformations. Nonetheless, the choice of the optimal support is still most often determined via empirical optimization, often with little associated insight into the detailed role of the support.

In the present work, we examine and clarify the role of the support in several key reactions related to the Rh-catalyzed Fischer−Tropsch (FT) synthesis[28,29] of ethanol (EtOH) from syngas.[30,31] Here, the choice of support is known to dramatically influence the activity and EtOH selectivity of the catalyst system,[15−18,32,33] leading in some cases to a significant increase in the EtOH yield.[15,32,33] Examining several key reactions and reaction intermediates with both silica and titania supports, we isolate the electronic and geometrical aspects of the metal−support interaction, and explain the experimentally observed selectivity trends in terms of these interactions. More broadly, we provide a general framework for predicting the influence of various oxide supports on elementary association/dissociation reactions in terms of electronic (charge transfer) and geometric (relaxation) effects.

Received: July 30, 2013
Revised: October 18, 2013
Published: October 23, 2013

   dx.doi.org/10.1021/cs4006277 | ACS Catal. 2013, 3, 2881−2890

2. METHODS

2.1. Model Systems. We study two common oxide supports, silica (SiO_2) and titania (TiO_2), with differing surface terminations representative of varying experimental conditions. Both supports are frequently utilized in experimental FT studies[33−37] and are representative of an irreducible and a reducible oxide support, respectively.[6,38] We also examine hydroxylated variants of both surfaces, which may occur during operating conditions because of water dissociation (silica) or hydrogen spillover (titania).

For the TiO_2 surface, the rutile form was used as this is the most common polymorph of TiO_2, and has been utilized extensively in catalytic research. We examined the energetically preferred (110) face,[39] yielding a set of hexa- and penta-coordinated Ti^{4+} atoms, with bridging oxygens (O_{br}) connecting the hexa-coordinated Ti^{4+} atoms. It has been shown that an odd number of Ti layers can lead to an overestimation of the TiO_2 surface energy,[40,41] therefore a TiO_2 surface composed of four layers of Ti atoms was used. In addition to the "clean" TiO_2 surface, we also considered a hydroxylated TiO_2 surface where hydrogens are adsorbed along the O_{br}.[15,39,42−44] Such a modification can arise from the effect of hydrogen spillover, whereby adsorbed H atoms migrate from the nanoparticle to support, partially reducing the surface Ti.[45] Henceforth, the clean surface will be referred to as TiO_2, and the hydroxlated surface is referred to as $(H)TiO_2$.

For the SiO_2 surface, the α-quartz polymorph was employed as it is the most common polymorph of SiO_2.[46] Density functional theory (DFT) calculations find that the (001) surface is the most stable[47] and reproduces the experimental 1 × 1 reconstruction.[47,48] For the current study, we employed the reconstructed surface of Goumans et al.,[47] which contains six layers of Si atoms. Given that water is a by product of the FT,[30,31] we also considered a modification whereby water has dissociatively adsorbed onto the surface, creating a series of geminal hydroxyl groups.[47,49,50] Henceforth, the clean surface will be referred to as SiO_2, and the hydroxylated surface is referred to as $(OH)(H)SiO_2$.

Turning to the nanoparticle model, we seek a *representative* model that incorporates many of the physical properties that are found under experimental conditions. Here we focus on Rh, as Rh has been shown to have a good selectivity to C_{2+} oxygenates in FT.[31] Transmission electron microscopy (TEM) experiments have found that the average size of a Rh nanoparticle is ∼2.5 nm,[36,51−59] with the lower end of the size distribution being ∼1.0 nm.[36,51,52,59] It is suspected that the preferential shape of the nanoparticle is the cuboctahedral shape, which has alternating (100) and (111) crystal facets.[60,61,61,62] Extended X-ray absorption fine structure (EXAFS)[52,63,64] and scanning tunneling microscopy (STM) studies[52,65] find that the nanoparticles preferentially form into a roughly hemispherical shape, with an average nanoparticle height of 0.4−0.5 nm[52,65] On the basis of these studies, we adopt a hemispherical three-layer cuboctahedral shape for our nanoparticle model, for a total of 37 Rh atoms. This produces a nanoparticle that is 1.5 × 1.0 nm at the base with a height of ∼0.4 nm, which is within the size distribution found by experiments. The Rh_{37} nanoparticle is shown schematically in Figure 1b, while the oxide-supported Rh_{37} nanoparticle is shown schematically in Figure 2. Note that since this nanoparticle model reproduces many of the properties of the corresponding bulk surface (vide infra), we expect that our results are fairly insensitive to the details of the nanoparticle model.

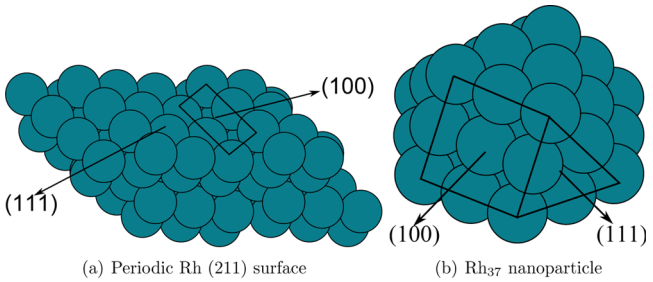

(a) Periodic Rh (211) surface (b) Rh_{37} nanoparticle

Figure 1. Graphical representations of the periodic Rh (211) surface and the Rh_{37} nanoparticle used the current study. The step edge is defined as the edge connecting the (100) and (111) facets.

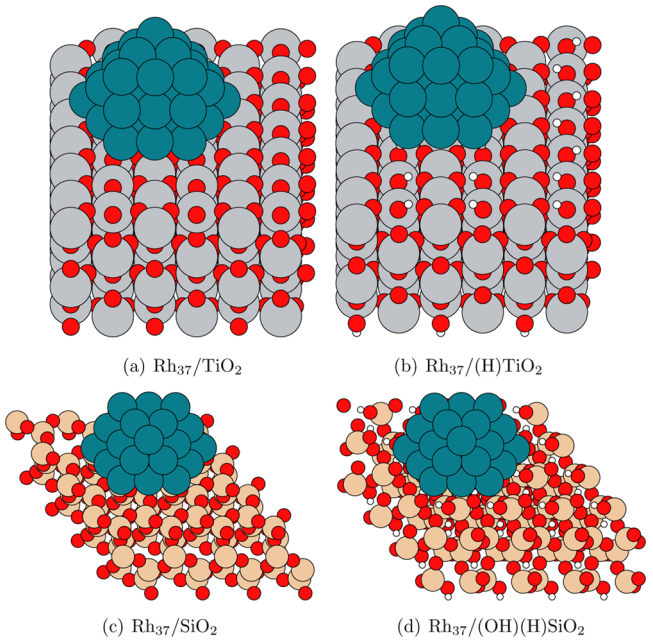

(a) Rh_{37}/TiO_2 (b) $Rh_{37}/(H)TiO_2$

(c) Rh_{37}/SiO_2 (d) $Rh_{37}/(OH)(H)SiO_2$

Figure 2. Graphical representations of the oxide-supported Rh_{37} nanoparticle used in the current study.

To isolate the geometric (relaxation) and electronic (charge transfer and/or "ligand" effects) aspects of the metal−support interactions, we consider two different nanoparticle geometries for each support surface. In the first model, the nanoparticle is held fixed in the unsupported nanoparticle geometry (henceforth rig-Rh_{37}), while in the second the nanoparticle is allowed to relax in the presence of the support (rel-Rh_{37}). In this way, a direct comparison can be made between the supported rig-Rh_{37} nanoparticle and the unsupported Rh_{37} nanoparticle, allowing us to isolate the electronic effects, while comparison with the rel-Rh_{37} nanoparticle allows us to isolate the geometrical effects caused by (local) relaxation of the nanoparticle by the support. Note that in both cases the nanoparticle is allowed to relax locally under the influence of any adsorbate before being deposited onto the support.

2.2. Reactions of Interest. Given the complexity of the FT reaction network,[30,31] a comprehensive study of the impact of support on all possible routes to EtOH production is prohibitive. Instead, we focus on those steps that have been previously identified as either rate or selectivity determining.[30,31] As such, we first examine the dissociation of an

dx.doi.org/10.1021/cs4006277 | ACS Catal. 2013, 3, 2881−2890

adsorbed carbon monoxide (CO) molecule into adsorbed C and O,

$$CO \rightarrow C + O \quad (1)$$

This reaction is well-studied on bulk Rh,[66−71] with a barrier approximately two times higher than the other processes, and is a crucial pathway to higher alkanes and oxygenates.

Furthermore, methane (CH_4) is a major undesirable byproduct of FT,[32,33,36,72] and understanding the role of the support in modulating selectivity toward EtOH vs methane is vital. Based on the FT pathways given in Mei et al.[30] and Chuang et al.[31] and microkinetic models of Rh surfaces,[71,73] the overall selectivity toward EtOH is determined by competition between hydrogenation of, and CO addition to, adsorbed CH_n. Based on prior DFT modeling, the lowest barriers for CH_n hydrogenation/insertion are when $n = 2$ or 3.[71,73] Thus we also examined the following selectivity-determining reactions:

$$CH_n + H \rightarrow CH_{n+1}, \quad n = 2, 3 \quad (2)$$

$$CH_n + CO \rightarrow CH_nCO, \quad n = 2, 3 \quad (3)$$

From eq 3, EtOH is produced by hydrogenation of the resulting CH_nCO species.

From these reactions, we have compiled a list of 10 key intermediates leading to EtOH, given in Table 1.

Table 1. Intermediates Considered in the Current Study

atomic species	molecular species	radical species
C	CO	CH_2
O	CH_2CO	CH_3
H	CH_4	CH_3CO

2.3. Computational Methods. The DFT calculations were performed within a locally modified version of the Atomistic Simulation Environment (ASE),[74] using the Vienna Ab Initio Software Package (VASP, version 4.6.36).[75−78] The Perdew−Burke−Ernzerhof (PBE) exchange-correlation functional[79] was employed with the core potentials represented via the projector augmented wave function (PAW) method of Blöchl[80] as modified by Kresse and Joubert.[81] Energies were minimized self-consistently using a 0.05 eV Gaussian smearing and mixture of the Davidson[82] and RMM−DIIS[83,84] algorithms, with a tight SCF convergence threshold of 10^{-6} eV. Calculations involving a bulk Rh surfaces utilized a 5 × 5 × 1 Monkhorst−Pack *k*-point mesh,[85] and all other calculations were performed at the Γ point. For the TiO_2 and $(H)TiO_2$ surfaces, we employed the DFT+*U* formalism of Dudarev et al.[86] in conjunction with a U_{eff} of 2.5 eV, which offers a good compromise between the reaction energies and band gap of titanium oxide species.[87] Note that we find that the *U* correction yields only modest corrections to the results presented herein.

The energy was minimized with respect to the ionic degrees of freedom by means of the fast inertial relaxation engine (FIRE),[88] as implemented in ASE, utilizing a force convergence criteria of 0.05 eV $Å^{-1}$. Optimizations were carried out without spin-polarization with a reduced (300 eV) plane-wave cutoff, while subsequent spin-polarized single-point energies (and thus all energy differences) were calculated using a 400 eV cutoff. Tests performed on a periodic Rh (111) surface with an adsorbed CO molecule and a rig-Rh_{37}/TiO_2 surface with an adsorbed atomic oxygen employing this scheme have shown there is a negligible impact on the final binding energies (<0.02 eV). We therefore conclude that the optimized geometries are negligibly affected by the reduced plane-wave cutoff, even for species with a relatively "hard" pseudopotentials (e.g., O).

3. RESULTS AND DISCUSSION

Using the computational model described above, we analyze the influence of metal−support interactions on the thermodynamics and kinetics of the above-identified rate and selectivity determining reactions. Since the associated change in reaction exothermicity can be directly related to the shift in the binding energies of the associated intermediates (see Section 3.2), we begin by examining these binding energy shifts upon a change in the oxide support and/or nanoparticle relaxation. We then rationalize these shifts in terms of charge transfer between oxide and nanoparticle using a simple model involving the bonding character of states around the Fermi level. Finally, we relate these binding energy shifts to the associated changes in reaction exothermicity (and rate), and discuss the implications for FT synthesis.

3.1. Binding Energies. We first define the binding energy of an adsorbate to a surface in the usual fashion,

$$E_{BE} = E_{surface-adsorbate} - E_{surface} - E_{adsorbate} \quad (4)$$

where $E_{surface-adsorbate}$ is the total energy of the surface plus the adsorbed molecule, $E_{surface}$ is the total energy of the bare surface, and $E_{adsorbate}$ is the total energy of the adsorbed molecule (in the adsorbate's gas-phase geometry); in this sign convention, a negative binding energy signifies an attractive interaction between adsorbate and surface. To isolate the most preferable binding sites for the adsorbates listed in Table 1, we examined a periodic Rh (211) surface. Similar to our Rh_{37} nanoparticle, the Rh (211) surface is composed of "terraces" made up of the (111) facet, with each terrace being connected to each other via a (100) facet. The Rh (211) surface prefers to bind species along the step edge between the (111) and (100) facets,[71] thus we explored various binding sites (such as the bridge, hollow, and top) along the step edge for the Rh_{37} nanoparticle. It should be noted that the nanoparticle contains different bridge and hollow sites: an upper and a lower site. The upper site is located near the top of the nanoparticle, between the second and third layers, while the lower site is located between the first and second layers. For the top site, we only considered the second layer; we found that the third (upper) layer of the nanoparticle typically binds adsorbates quite weakly (with an E_{BE} less than 25% of the step edge), while adsorption on the first layer may contain *direct* interactions between adsorbate and support (an effect which we leave as the subject for a future study). For the CH_nCO adsorbates, we observe that the binding is through two binding sites: the carbonyl group is located on a top site, while the CH_n fragments are located on a neighboring bridge site. We thus denote these species via the binding site of the associated CH_n group.

A comparison between the binding energies on Rh (211) and Rh_{37} (for the same local adsorption geometry) is given in Table 2. Note that the preferred binding sites for both systems are qualitatively similar, that is, either along a step edge between the (100) and (111) facets, or at a nearby hollow site. Differences in binding energies are also very modest (typically < 0.1 eV), although larger differences are observed for the strongly adsorbed C/O atoms and CH_2. These differences most likely arise from changes in the metal d-states upon moving from the periodic surface to a finite sized nanoparticle.[67,89−91] For the atomic species, we also note that there is a preference

dx.doi.org/10.1021/cs4006277 | ACS Catal. 2013, 3, 2881−2890

Table 2. Binding Energies (E_{BE}) for the Various Adsorbates on a Rh (211) Surface and a Rh_{37} Nanoparticle (eV)

			Rh_{37}	
adsorbate	binding site	Rh (211)	lower	higher
CO	top[a]	−1.97	−2.00	
C	(100) hollow	−7.12	−7.64	−7.66
O	(111) hollow	−5.46	−4.94	−5.18
H	bridge	−2.72	−2.75	−2.66
CH_2	bridge	−4.33	−4.52	−4.39
CH_3	top[a]	−1.94	−2.05	
CH_3	bridge	−2.17	−2.12	−2.14
CH_2CO[b]	bridge	−1.57	−1.71	−1.70
CH_3CO[b]	bridge	−2.67	−2.69	−2.18

[a]For the Rh_{37} nanoparticle there was only one top site of interest. [b]For these species the upper and lower sites denote the location where the CH_n fragment is located.

for the upper sites on the Rh_{37} nanoparticle (i.e., the upper bridge site for the hydrogen atom, hollows for the C and O atoms). On the basis of these observations, we will take as the most stable binding sites for the Rh_{37} nanoparticle those that are analogous to binding sites on the Rh (211) surface.

3.1.1. Supported Rh_{37} Nanoparticle. Before turning to the supported nanoparticles, we note that it is more profitable to consider *shifts* in the binding energies induced by the support rather than absolute binding energies, since the former can be trivially related to corresponding shifts in the reaction thermodynamics (see Section 3.2). We define the shift in the binding energy (ΔE_{BE}) between the supported Rh_{37} nanoparticle and the unsupported Rh_{37} nanoparticle as

$$\Delta E_{BE} = E_{BE}^{supported} - E_{BE}^{unsupported} \quad (5)$$

As such, a negative ΔE_{BE} corresponds to an adsorbate binding more strongly to the oxide-supported nanoparticle.

SiO_2 and (OH)(H)SiO_2 Supports. The ΔE_{BE}'s for the adsorbates listed in Table 1 interacting with the SiO_2 and (OH)(H)SiO_2 supported rig-Rh_{37} and rel-Rh_{37} nanoparticles are given in Table 3. Examining the shifts for the rig-Rh_{37}/SiO_2 model, we see that the electronic support effects for SiO_2 are quite small, 0.11 eV or less in magnitude for the lower bridge and hollow sites. For the upper bridge and hollow sites, we do see a moderate shift to weaker binding for the strongly interacting C, H, and CH_2CO species, and a larger shift to stronger binding for the O atom; however the remaining species show an insignificant shift in the binding energies. Hydroxylation of the SiO_2 surface (i.e., rig-Rh_{37}/(OH)(H)-SiO_2) does not significantly change the above results—most binding energies change by less than 0.10 eV when going from the rig-Rh_{37}/SiO_2 surface to the rig-Rh_{37}/(OH)(H)SiO_2 surface.

However, upon relaxation to the rel-Rh_{37}/SiO_2 and rel-Rh_{37}/(OH)(H)SiO_2 surfaces we do find some modest changes to the binding energies. Generally, relaxation leads to binding energy shifts that are systematically more negative (attractive) by ∼0.1−0.3 eV. We attribute this to an increased Rh−Rh bond length upon relaxation, decreasing the coordination of Rh atoms and thus increasing the adsorbate−Rh_{37} binding in conjunction with the bond order conservation model.[92] Overall, we conclude for the silica-based supports that relaxation effects caused by the presence of the support are more important than the electronic effects, and that the influence of the support overall is modest. This is in good accord with the conventional viewpoint of silica as an inert support.[38] Nonetheless, it is important to point out that the binding energies of very strongly adsorbed (particularly atomic) species are still slightly perturbed by the metal−support interaction. Although the resulting support-induced binding energy shifts are small relative to the total binding energy, these shifts are quite large on an absolute scale (several tenths of an eV), and thus may induce nontrivial influences on reactions which involve such reactants/products/intermediates (see Section 3.2).

Table 3. Changes in Binding Energies (ΔE_{BE})[a] for the Various Adsorbates with a Silica (SiO_2) Based Support (eV)

	Rh_{37}/SiO_2		Rh_{37}/(OH)(H)SiO_2	
adsorbate	rigid	relaxed	rigid	relaxed
		Top		
CO	−0.01	−0.10	0.02	−0.09
CH_3	0.09	−0.16	0.06	−0.08
		Low		
C	0.04	−0.18	0.05	−0.12
O	0.08	−0.17	0.08	−0.14
H	0.11	−0.25	−0.08	−0.23
	0.02	−0.06	0.01	−0.03
CH_3	0.06	−0.09	0.02	−0.06
CH_4	0.07	0.00	0.07	0.01
CH_2CO	0.07	−0.08	0.07	−0.03
CH3CO	0.05	−0.18	0.01	−0.14
		High		
C	0.13	−0.15	0.06	−0.10
O	−0.18	−0.45	−0.19	−0.40
H	0.11	−0.11	0.07	−0.09
CH_2	0.05	−0.08	0.04	−0.04
CH_3	0.02	−0.06	0.02	−0.06
CH_4	0.06	−0.02	0.04	−0.01
CH_2CO	0.16	0.02	0.10	0.05
CH_3CO	0.05	−0.12	−0.04	−0.13

[a]Change in binding energy defined such that $E_{BE}^{supported} = E_{BE}^{unsupported} + \Delta E_{BE}$.

TiO_2 and (H)TiO_2 Supports. The ΔE_{BE}'s for the adsorbates listed in Table 1 interacting with the TiO_2 and (H)TiO_2 supported rig-Rh_{37} and rel-Rh_{37} nanoparticles are given in Table 4. Examining the ΔE_{BE}'s for the rig-Rh_{37}/TiO_2 surface, it is immediately apparent that the electronic influence of the TiO_2 support tends to (sometimes considerably) strengthen the adsorbate−Rh_{37} binding, with this effect generally more significant for the lower bridge and hollow sites than for the upper bridge and hollow sites. While this effect is fairly modest for the molecular, H, and CH_3CO species (with a $\Delta E_{BE} \leq 0.11$ eV), we see a much stronger electronic support effect for the remaining species, with a ΔE_{BE} between −0.24 and −0.35 eV for the lower binding sites; for the upper binding sites the stronger binding is generally <0.10 eV, with the exception of C and O; here the binding energy is stronger by 0.29 and 0.49 eV in magnitude, respectively.

Upon relaxation to the rel-Rh_{37}/TiO_2 surface, these trends are enhanced as adsorbates are further stabilized relative to the unsupported nanoparticle. Similar to the SiO_2 and (OH)(H)-SiO_2 supports, we attribute this enhancement to the lengthened Rh−Rh bonds in the Rh_{37} nanoparticle, in addition to a slight flexing of the bottom Rh layer. Both of these effects cause decreased Rh coordination, which in turns increases the binding strength. Generally speaking, the effect of the relaxation contributes 0.1−0.2 eV in magnitude; however we found a

dx.doi.org/10.1021/cs4006277 | ACS Catal. 2013, 3, 2881−2890

Table 4. Changes in Binding Energies (ΔE_{BE})[a] for the Various Adsorbates with a Titania (TiO_2) Based Support (eV)

	Rh_{37}/TiO_2		$Rh_{37}/(H)TiO_2$	
adsorbate	rigid	relaxed	rigid	relaxed
		Top		
CO	−0.11	−0.16	0.06	−0.15
CH_3	−0.04	−0.11	0.22	−0.06
		Low		
C	−0.35	−0.41	0.13	−0.16
O	−0.23	−0.22	−0.02	−0.32
H	−0.05	−0.41	0.20	−0.12
CH_2	−0.24	−0.39	0.07	0.04
CH_3	−0.36	−0.41	0.15	0.03
CH_4	0.03	0.00	0.07	−0.10
CH_2CO	−0.11	−0.09	0.01	−0.07
CH_3CO	−0.11	−0.74	0.09	−0.17
		High		
C	−0.29	−0.53	0.10	−0.17
O	−0.49	−0.75	−0.22	−0.51
H	−0.08	−0.17	0.15	−0.12
CH_2	−0.02	−0.08	0.07	−0.05
CH_3	−0.08	−0.22	0.07	−0.06
CH_4	0.03	−0.10	0.02	0.01
CH_2CO	0.22	0.01	0.21	0.01
CH_3CO	−0.02	−0.17	0.01	−0.16

[a]Change in binding energy defined such that $E_{BE}^{supported} = E_{BE}^{unsupported} + \Delta E_{BE}$.

much higher relaxation effect for the H species at the lower bridge site and for the CH_3CO species at the upper bridge sites. *Overall, considering both electronic and geometric effects, these sizable binding energy shifts portend significant changes to the associated thermochemistry and kinetics.*

We also explore the corresponding hydroxlated titania surfaces. Such hydroxyl termination may arise under reaction condition from spillover of atomic hydrogen from the nanoparticle to the support, formally reducing the Ti atoms and generating surface hydroxyl groups. In contrast to the rig-Rh_{37}/TiO_2 surface, for the rig-$Rh_{37}/(H)TiO_2$ surface we see a trend of weaker binding under the electronic influence of the support. The electronic contribution is fairly moderate, around 0.2 eV or less in magnitude. Relaxation to the rel-$Rh_{37}/(H)TiO_2$ surface, tends to counteract this trend, with the relaxation tending to stabilize adsorbates by 0.1−0.3 eV. Here, the electronic and geometric metal−support interactions tend to cancel, yielding (on average) a small net attractive shift in typical binding energies.

Looking across the various oxide supports and surface terminations, we find that the *geometric* contribution to the metal−support interaction yields a fairly consistent stabilizing influence of 0.1−0.3 eV to the binding of adsorbates. Since this geometric effect is governed by the local relaxation of the nanoparticle, it depends only indirectly on the detailed chemical composition of the underlying oxide support. In contrast, we find that the *electronic* contribution to the metal−support interaction is highly variable in both magnitude and sign, and depends sensitively on both the composition and termination of the underlying oxide. We hypothesize that the preponderance of this electronic effect arises from charge transfer between metal and nanoparticle.

Performing a Bader charge analysis[93,94] and summing the resulting Bader charges over the Rh_{37} nanoparticle, we can extract the total number of electrons transferred either to or from the oxide surface. These results are presented in Table 5.

Table 5. Charge (e^-) for the Rh_{37} Nanoparticle on the Various Oxide Supports

	Rh_{37}/TiO_2		$Rh_{37}/(H)TiO_2$	
	rigid	relaxed	rigid	relaxed
Q_{NP}	2.83	2.65	−1.40	−1.42
	Rh_{37}/SiO_2		$Rh_{37}/(OH)(H)SiO_2$	
	rigid	relaxed	rigid	relaxed
Q_{NP}	0.27	0.25	0.20	0.20

For the silica surfaces, we find only a small net transfer of charge from the nanoparticle to the surface (∼ 0.25 e^-) for both the rigid and the relaxed nanoparticles. This is to be expected as silica is conventionally considered a "neutral" support in terms of its Lewis acidity/basicity,[38] and the binding energy shifts for the SiO_2 and $(OH)(H)SiO_2$ surfaces are fairly small. In contrast, for the TiO_2 based supports we find a significant amount of charge has been transferred between the nanoparticle and the support. For the clean TiO_2 support, 2.83 and 2.64 electrons are transferred to the oxide support for rigid and relaxed nanoparticles, respectively. On the basis of a charge density difference analysis, we find that these electrons are donated to the 2p surface states of the O_{br}. This is further supported by the Bader charge analysis which shows O_{br} in contact with the nanoparticle gaining about ∼0.16 electrons each. For the hydroxylated $(H)TiO_2$ surface, charge density difference analysis shows additional density transferred *to* the Rh_{37} nanoparticle, originating from Ti_{6c} d-states and from the surface hydroxyls. This results in ∼1.40 electrons transferred from the $(H)TiO_2$ support to nanoparticle. The charge density differences for the rig-Rh_{37}/TiO_2 and rig-$Rh_{37}/(H)TiO_2$ surfaces are shown in the Supporting Information, Figure S1.

These results are both consistent with the anticipated Lewis acid/base properties of the oxide support, and confirmed by prior XPS observations. Irreducible oxides like silica feature low-lying valence and high-lying conduction bands, yielding Lewis neutral behavior and minimal charge transfer between support and metal, and is thus characteristic of the silica support's innocent behavior. In contrast, reducible oxides, such as TiO_2, often act as a weak Lewis acid, accepting electron density because of the residual oxidizing power of the surface oxygens.[6,7] Hydrogen spillover introduces hydroxyl groups to the surface, which act as Lewis basic centers, donating electron density.[7] In addition, prior XPS studies of Rh/TiO_2[15−18,63] have shown that the Rh $3d_{5/2}$ peak shifts up in energy with respect to the bulk, consistent with positive charging of the nanoparticle. The introduction of surface hydroxyl groups (such as those found on the $(H)TiO_2$ support) has been found to yield negative peak shifts, indicative of negative charging.[8,14,15]

To understand the effect of the charge state of the nanoparticle on adsorbate binding, we applied a charge to the unsupported Rh_{37} nanoparticle that approximately corresponds with the charge found on the supported nanoparticles from the Bader charge analysis, and then recalculated the binding energy of the various adsorbates. It should be noted that since the nanoparticle has metallic character, the charge on the

dx.doi.org/10.1021/cs4006277 | ACS Catal. 2013, 3, 2881−2890

unsupported nanoparticle will be distributed largely uniformly across the entire nanoparticle, whereas charge transfer from the supported nanoparticle was dominated by the bottom of the nanoparticle; however, we believe the model still provides qualitative insight into the role of nanoparticle charge. We focus on the lower binding sites and top site, as those sites showed the most significant changes in the binding energies. The results of the charge model are given in Table 6. Overall, it is clear that

Table 6. Changes in the Binding Energies (ΔE_{BE}) for the Various Adsorbates with Varying Nanoparticle Charge (eV)[a]

adsorbate	Rh_{37}^{+3}	Rh_{37}/TiO_2	Rh_{37}^{-2}	$Rh_{37}/(H)TiO_2$
CO	0.00	−0.11	−0.05	0.06
CH_3	−0.19	−0.04	0.07	0.22
C	−0.06	−0.35	−0.07	0.13
O	0.33	−0.23	0.11	−0.02
H	−0.26	−0.05	−0.10	0.20
CH_2	−0.21	−0.24	0.07	0.07
CH_3	−0.33	−0.36	0.12	0.15
CH_2CO	−0.07	−0.11	0.05	0.01
CH_3CO	−0.35	−0.11	0.13	0.09

[a]Adsorbate geometries are as in Table 2.

positive charging yields stronger adsorbate−metal binding, while negative charging results in a weaker adsorbate−metal binding. With the exception of the atomic species, the directionality (and many times, the magnitude) of the change in the binding energies are in good agreement with the trends in the binding energy shifts observed with the explicit TiO_2 and $(H)TiO_2$ supported rig-Rh_{37} nanoparticle.

To probe the mechanism by which nanoparticle charging yields systematic shifts in adsorbate binding, we performed a balanced crystal orbital overlap population (BCOOP)[95,96] analysis using Kohn−Sham orbitals from VASP projected onto an atom-centered Gaussian basis set.[97−99] The BCOOP analysis yields the bonding and antibonding character of particular regions within the density of states (DOS), with bonding and antibonding contributions denoted as positive and negative, respectively. A representative BCOOP curve for CH_3 adsorbed onto a top site of the Rh_{37} nanoparticle is given in Figure 3. In general, from the BCOOP analysis we find that the DOS around the Fermi level are primarily antibonding (with respect to the metal-adsorbate bond) in nature. Adding (inducing a negative charge state) or removing (inducing a positive charge state) electrons from the nanoparticle shifts the Fermi level, thus populating or depopulating antibonding adsorption states. As such, positive nanoparticle charging depopulates antibonding states around the Fermi level, which would in turn yields stronger binding between the adsorbate and the Rh_{37} nanoparticle, while negative charging has the opposite effect.

Certainly this crude model is incomplete, as can be seen from the failure of the charge model to at least qualitatively predict the change in binding energies for the strongly interacting atomic species. Examining the various moments from the density of states for the unsupported and supported nanoparticles, we also see that the s and p bands of the latter are broadened comparatively because of the interactions with surface 2p orbitals from the oxygens on the support (see Supporting Information, Table S3). Note that we find a negligible change in the d-band moments of the Rh_{37} nanoparticle, and thus we believe that the contributions to

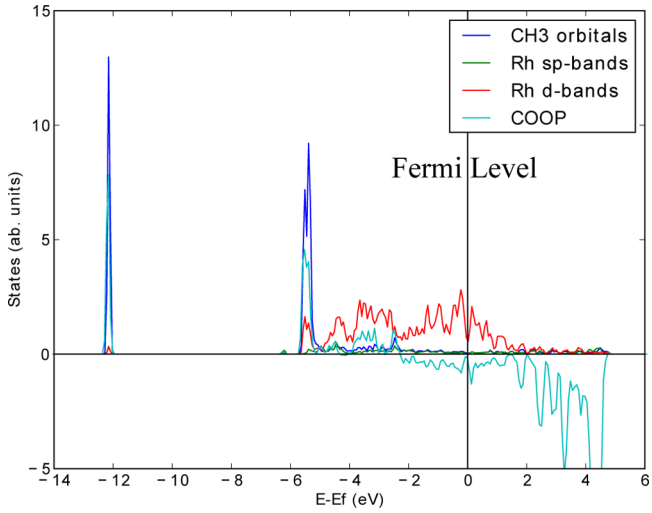

Figure 3. COOP analysis of CH_3 adsorbed onto a top site. Bands with are bonding and antibonding with respect to the metal-adsorbate are given as positive and negative, respectively.

the change in the binding energies because of this broadening play a larger role for the atomic species than the effects of charge transfer.

3.2. Thermodynamic and Kinetic Consequences. Support-induced binding energy shifts of reactants, products, and intermediates will significantly impact associated reaction thermodynamics and kinetics. Using Hess' Law, we can write the reaction energy (ΔE_{rxn}) for a particular surface reaction as

$$\Delta E_{rxn} = \Delta E_{rxn}^{gas-phase} + \sum_{i=1}^{N_{products}} E_{BE}(product_i) - \sum_{j=1}^{N_{reactants}} E_{BE}(reactant_j) \quad (6)$$

where $\Delta E_{rxn}^{gas-phase}$ is the gas-phase reaction energy for the reaction in question. However, a more useful measure of the support's impact on the ΔE_{rxn}'s is to consider a $\Delta\Delta E_{rxn}$ between the unsupported and oxide-supported Rh_{37} nanoparticle, that is, the change in the reaction energy induced by the metal−support interaction,

$$\Delta\Delta E_{rxn} = \Delta E_{rxn}^{supported} - \Delta E_{rxn}^{unsupported} \quad (7)$$

The $\Delta\Delta E_{rxn}$ for a particular reaction can then be expressed, in turn, in terms of the associated binding energy shifts of the reactants and products,

$$\Delta\Delta E_{rxn} = \sum_{i=1}^{N_{products}} \Delta E_{BE}(product_i) - \sum_{j=1}^{N_{reactants}} \Delta E_{BE}(reactant_j) \quad (8)$$

where ΔE_{BE} is defined in eq 5, with the ΔE_{BE}'s taken from Tables 4 and 3. For eq 8, we use the ΔE_{BE}'s for only the most stable binding sites (i.e., the high site for the atomic species, and the low/top sites for the remaining species).

SiO_2 and $(OH)(H)SiO_2$ Supports. The rig-Rh_{37}/SiO_2 and rig-$Rh_{37}/(OH)(H)SiO_2$ surfaces generally exhibit almost negligible ΔE_{BE}'s, indicating a very small electronic support effect, and yielding only small changes in the $\Delta\Delta E$'s, less than 0.10 eV in magnitude (see Table 7). However, upon relaxation to the rel-Rh_{37}/SiO_2 and rel-$Rh_{37}/(OH)(H)SiO_2$ surfaces, we see more

dx.doi.org/10.1021/cs4006277 | ACS Catal. 2013, 3, 2881−2890

Table 7. ΔE_{rxn} for the Rh_{37} Nanoparticle and Changes in Reaction Energies ($\Delta\Delta E_{rxn}$) for the Various Reactions with a Silica (SiO_2) Based Support (eV)

		$\Delta\Delta E_{rxn}$			
	ΔE_{rxn}	Rh_{37}/SiO_2		$Rh_{37}/(OH)(H)SiO_2$	
adsorbate	Rh_{37}	rigid	relaxed	rigid	relaxed
$CO \rightarrow C + O$	0.82	−0.04	0.50	−0.15	−0.41
$CH_2 + H \rightarrow CH_3$	0.06	−0.07	0.08	−0.06	0.06
$CH_3 + H \rightarrow CH_4$	−0.02	−0.10	0.20	−0.02	0.16
$CH_2 + CO \rightarrow CH_2CO$	0.70	0.06	0.08	0.04	0.09
$CH_3 + CO \rightarrow CH_3CO$	0.33	0.00	0.01	−0.03	0.01

substantial shifts in the reaction energies, particularly for reactions involving atomic reactants/products. From Table 3, it is these atomic species that are most significantly affected by the metal−support interaction. In particular, for rel-Rh_{37}/SiO_2 and rel-$Rh_{37}/(OH)(H)SiO_2$ we see an increase in the exothermicity for the CO dissociation reaction eq 1 with $\Delta\Delta E_{rxn}$'s of −0.50 and −0.41 eV, respectively. This is attributed to the stronger binding for the atomic species induced by the relaxation of the nanoparticle in the presence of the support. For methane production (eq 2), we see an increase in the endothermicity of 0.20 and 0.16 eV for the rel-Rh_{37}/SiO_2 and rel-$Rh_{37}/(OH)(H)SiO_2$ surfaces, respectively.

While we reserve detailed discussion of the impact of these shifts to the *overall* EtOH selectivity to section Section 3.3, it is important to note that these significant shifts correspond to a change of tens of kJ mol^{-1} in the exothermicity of these elementary steps, and thus significant changes to the equilibrium of these elementary steps, even for an "innocent" silica support. Perhaps even more important, because of the well-known Brønsted−Evans−Polyani (BEP) relationship,[68,100−103] these shifts also portend potentially significant changes to the kinetics of the elementary steps, with increased exothermicity tending to lower reaction barriers and enhance rates. As such, we would anticipate enhancement in the CO dissociation process, and a slight decrease in the rate of methane formation.

TiO_2 and (H)TiO_2 Supports. From Table 4, recall that TiO_2 tends to induce stronger adsorbate binding, further accentuated upon relaxation of the nanoparticle. Thus, from eq 8, dissociation reactions (yielding more adsorbed products than reactants) will generally become more thermodynamically favorable (i.e., more exothermic), while association reactions generally become less favorable. Looking at the detailed $\Delta\Delta E$'s for TiO_2 (see Table 8), it is apparent that this trend holds in almost all cases. Focusing specifically on the rel-Rh_{37}/TiO_2 system, note that the thermodynamics of the CO dissociation, methane formation, and CO addition to methylene reactions all undergo significant shifts consistent with this trend, with the former become more exothermic by over 1 eV. The one notable exception is CO addition to methyl, which (for the relaxed nanoparticle) becomes somewhat more exothermic. On the basis of the BEP relations, these results suggest significant changes in the kinetics of the associated elementary steps, with potentially significant implications on overall EtOH selectivity. The implications of these results for FT are discussed in detail in Section 3.3.

Table 8. ΔE_{rxn} for the Rh_{37} Nanoparticle and Changes in Reaction Energies ($\Delta\Delta E_{rxn}$) for the Various Reactions with a Titania (TiO_2) Based Support (eV)

		$\Delta\Delta E_{rxn}$			
	ΔE_{rxn}	Rh_{37}/TiO_2		$Rh_{37}/(OH)(H)TiO_2$	
reaction	Rh_{37}	rigid	relaxed	rigid	relaxed
$CO \rightarrow C + O$	0.82	−0.67	−0.12	−0.18	−0.53
$CH_2 + H \rightarrow CH_3$	0.06	−0.04	0.15	−0.07	0.11
$CH_3 + H \rightarrow CH_4$	−0.02	0.47	0.58	−0.23	−0.01
$CH_2 + CO \rightarrow CH_2CO$	0.70	0.24	0.46	−0.12	0.04
$CH_3 + CO \rightarrow CH_3CO$	0.33	0.36	−0.17	−0.12	−0.05

As expected, shifts in reaction energies on the corresponding hydroxylated surfaces are far more modest, consistent with the modest binding energy shifts on $(H)TiO_2$ given in Table 4. Because of the electronic metal−support interaction, general trends for the rig-$Rh_{37}/(H)TiO_2$ model are the opposite of the above, with association reactions becoming slightly more exothermic. However, CO dissociation, too, becomes (slightly) more exothermic, in contrast to qualitative expectations. Incorporation of relaxation largely opposes the electronic metal−support interaction, further moderating the shifts in binding energy and the resulting changes to reaction exothermicity.

3.3. Implications for FT Synthesis. The above results clearly demonstrate that the metal−support interaction can induce significant changes to adsorption energies, and therefore to the thermodynamics and kinetics of elementary processes. Although we have shown explicit results for a variety of reactants, intermediates, and products of relevance to FT, the implications on the overall EtOH selectivity are a priori unclear. To this end, previous detailed microkinetic modeling has shown that EtOH selectivity is determined largely by a competition between H and CO addition to the surface adsorbed CH_3.[73] As such, we will focus our discussion on the influence of the support on these two crucial competing processes.

For the addition of H to CH_3, silica support (independent of surface termination) reduces the exothermicity of the hydrogenation by approximately 0.2 eV, which will tend to slightly shift equilibrium away from methane formation. Kinetically, we expect only modest changes based on the change in exothermicity; assuming a moderate α value (<0.5) for the association reaction,[103,104] a BEP relation would predict only very small changes to the associated activation energy. Furthermore, silica has essentially no impact on the thermodynamics or kinetics of the CO addition to methyl. We thus conclude that silica has little impact on the determination of the selectivity for the final products. Note, however, that given the significant changes in the CO dissociation thermodynamics (and likely kinetics, as well), the overall *activity* of the catalyst may be nontrivially enhanced via the metal-silica interaction.

dx.doi.org/10.1021/cs4006277 | ACS Catal. 2013, 3, 2881−2890

This picture changes dramatically for the TiO_2 support. For the TiO_2, a combination of electronic and geometric effects reduced the exothermicity of H addition by 0.58 eV. If we assume a $\alpha \approx 0.3$,[104] BEP relations would predict an increase in the associated activation energy of ∼0.2 eV. From their microkinetic model, Choi and Liu find that such increases in barriers yields ∼50% increase in EtOH selectivity.[73] Furthermore, we find that CO addition to CH_3 is favored by an additional −0.17 eV on TiO_2. Using a similar analysis, microkinetic modeling predicts a further slight increase in EtOH selectivity.[73] In contrast, hydroxylation to $(H)TiO_2$ largely mitigates both these effects, yielding a fairly "inert" support that is much similar to silica in terms of its effect on selectivity.

These observations are consistent with prior experimental observations of silica-[30,32,33,72,105] and titania-[33,63,106−108] supported Rh nanoparticles, where it is observed that the former exhibits greater methane selectivity on average. Furthermore, a direct comparison between the silica- and titania-supported catalysts have shown a slight decrease in methane selectivity and a dramatic increase (from zero to ∼30%) in C_{2+} oxygenate formation (including an 11% increase in EtOH yield) for the latter.[33] These observed support-induced selectivity modifications are substantial, although somewhat smaller than would be expected based on the above analysis. This is likely due to a combination of factors, including the presence of additional C_{2+} oxygenate products (not included in the prior analysis), partial spillover-induced TiO_2 hydroxylation under reaction conditions, and/or lateral adsorbate−adsorbate interactions. Although our model focuses on the low-pressure regime (with isolated adsorbates), we do not anticipate that inclusion of lateral interactions would qualitatively change the above trends since the fundamental geometric and electronic aspects of the metal−support interaction are largely independent of adsorbate coverage. Thus, while a more complex model (e.g., accounting for coverage-dependent CO binding energies[109−112]) would likely offer enhanced *quantitative* accuracy, our analysis is nonetheless able to clearly attribute these selectivity changes to a combination of support-induced charge transfer and nanoparticle relaxation, leading to significant changes in adsorbate binding and thus reaction thermodynamics and kinetics.

4. CONCLUSIONS

Metal oxides are ubiquitous as support materials for metal nanoparticles in heterogeneous catalysis, and we have shown how the resulting metal−support interaction can yield *significant* modifications to the binding of adsorbates to a representative Rh nanoparticle. Taking FT synthesis of ethanol (EtOH) as a representative example, we examined the influence of common silica and titania supports. We have found that a silica-based support has little effect over the binding energies when compared to the unsupported Rh_{37} nanoparticle, while a titania-based support yields considerable changes. Decoupling the electronic and geometric aspects of the metal−support interaction, we find that geometric relaxation of the nanoparticle because of the presence of the oxide support yields a fairly systematic *increase* in adsorbate binding by ∼0.1−0.3 eV, independent of the nature of oxide, because of relaxation-induced strain and increasing metal−metal bond distances. In contrast, the electronic contribution to the metal−support interaction is far more sensitive to the composition and termination of the oxide. We are able to rationalize the latter in terms of charge transfer between support and nanoparticle. Here, Lewis-neutral silica yields little charge transfer, and thus little electronic support effect, whereas the TiO_2 and the hydroxylated $(H)TiO_2$ supports lead to a positive and a negative nanoparticle charging, respectively. In turn, nanoparticle charging modulates the adsorption energies by populating or depopulating states of antibonding character around the Fermi level. Crucially, these (sometimes significant) shifts in adsorbate binding energies induce corresponding changes to the reaction thermodynamics and kinetics for elementary steps involving these adsorbed species.

For the specific case of FT, we showed how the metal−support interaction can be exploited to influence the EtOH selectivity over methane. On the basis of the microkinetic model of Choi and Liu,[73] we can conclude that the overall selectivity toward EtOH production on the TiO_2 support is due to the increased activation energy for the final hydrogenation step leading to methane, coupled with a small decrease in the activation energy for CH_3 insertion into CO. In contrast, silica yields only modest changes to these important selectivity determining steps.

Although our quantitative results have focused on FT, support effects are ubiquitous in heterogeneous catalysis. More generally, the above ideas can be used to crudely predict the influence of a support even in the absence of detailed calculations. From eq 8, if $N_{products} > N_{reactants}$ (e.g., a dissociation reaction), and the oxide support tends to induce stronger adsorbate binding (e.g., TiO_2), then the support will tend to increase the exothermicity of the corresponding elementary step. Similarly, such a support would tend to decrease the exothermicity of association reactions. The tendency of a particular support to induce stronger/weaker adsorption is dictated by the metal−support interaction, factors which can be considered quite generally without regard to the details of any particular catalytic transformation.

A complete picture of metal−support interactions is certainly complex, and may also include direct catalysis by the oxide,[113,114] reactions at the metal−support interface,[23−27] or nanoparticle morphology.[8,51,52,60,62,115,116] Nonetheless, the present study provides a detailed picture of the influence of common silica and titania supports on the reactivity of supported metal nanoparticles, and a decoupling of the metal−support interaction into electronic and geometric components. As such, it also provides some initial steps toward a more rational and less empirical selection of oxide supports to optimize reaction activity and selectivity.

■ ASSOCIATED CONTENT

Supporting Information

Charge density differences for the Rh_{37} nanoparticle adsorbed onto the TiO_2 and $(H)TiO_2$ support surfaces; absolute binding energies for adsorbates on supported nanoparticles; band energies and widths for supported nanoparticles. This material is available free of charge via the Internet at http://pubs.acs.org.

■ AUTHOR INFORMATION

Corresponding Author

*E-mail: schmidt@chem.wisc.edu.

Notes

The authors declare no competing financial interest.

■ ACKNOWLEDGMENTS

We would like to thank Mr. Benjamin Dunnington and Prof. Wissam al-Saidi for several useful discussions. Computational resources for this work come from the Extreme Science and Engineering Discovery Environment (XSEDE), under National Science Foundation Grant OCI-1053575. Acknowledgment is made to the Donors of the American Chemical Society Petroleum Research Fund for support of this research. J.R.S. is an Alfred P. Sloan Research Fellow.

■ REFERENCES

(1) van Santen, R.; Neurock, M. *Molecular Heterogeneous Catalysis*; Wiley-VCH: Weinheim, Germany, 2006.
(2) Freund, H.; Kuhlenbeck, H.; Libuda, J.; Rupprechter, G.; Bäumer, M.; Hamann, H. *Top. Catal.* **2001**, *15*, 201−209.
(3) Tauster, S. J.; Fung, S. C.; Garten, R. L. *J. Am. Chem. Soc.* **1978**, *100*, 170−175.
(4) Tauster, S. J. *Acc. Chem. Res.* **1987**, *20*, 389−394.
(5) Campbell, C. T. *Nat. Chem.* **2012**, *4*, 597−598.
(6) Pacchioni, G. *Phys. Chem. Chem. Phys.* **2013**, *15*, 1737−1757.
(7) Metiu, H.; Chrétien, S.; Hu, Z.; Li, B.; Sun, X. *J. Phys. Chem. C* **2012**, *116*, 10439−10450.
(8) Cárdenas-Lizana, F.; Hao, Y.; Crespo-Quesada, M.; Yuranov, I.; Wang, X.; Keane, M. A.; Kiwi-Minsker, L. *ACS Catal.* **2013**, *3*, 1386−1396.
(9) Wörz, A. S.; Heiz, U.; Cinquini, F.; Pacchioni, G. *J. Phys. Chem. B* **2005**, *109*, 18418−18426.
(10) Carrasco, J.; Barrio, L.; Liu, P.; Rodriguez, J. A.; Ganduglia-Pirovano, M. V. *J. Phys. Chem. C* **2013**, *117*, 8241−8250.
(11) Mpourmpakis, G.; Vlachos, D. G. *J. Phys. Chem. C* **2009**, *113*, 7329−7335.
(12) Jung, J.; Shin, H.-J.; Kim, Y.; Kawai, M. *J. Am. Chem. Soc.* **2012**, *134*, 10554−10561.
(13) Kim, H. Y.; Lee, H. M.; Henkelman, G. *J. Am. Chem. Soc.* **2012**, *134*, 1560−1570.
(14) Larichev, Y. V.; Moroz, B. L.; Bukhtiyarov, V. I. *Appl. Surf. Sci.* **2011**, *258*, 1541−1550.
(15) Linsmeier, C.; Taglauer, E. *Appl. Catal., A* **2011**, *391*, 175−186.
(16) Talo, a.; Lahtinen, J.; Hautojärvi, P. *Appl. Catal., B* **1995**, *5*, 221−231.
(17) Labich, S.; Taglauer, E.; Knözinger, H. *Top. Catal.* **2001**, *14*, 153−161.
(18) Óvári, L.; Kiss, J. *Appl. Surf. Sci.* **2006**, *252*, 8624−8629.
(19) Kitchin, J. R.; Nørskov, J. K.; Barteau, M. a.; Chen, J. G. *J. Chem. Phys.* **2004**, *120*, 10240−10246.
(20) Kitchin, J.; Nørskov, J.; Barteau, M.; Chen, J. *Phys. Rev. Lett.* **2004**, *93*, 4−7.
(21) Nørskov, J. K.; Bligaard, T.; Rossmeisl, J.; Christensen, C. H. *Nat. Chem.* **2009**, *1*, 37−46.
(22) Nørskov, J. K.; Abild-Pedersen, F.; Studt, F.; Bligaard, T. *Proc. Natl. Acad. Sci. U. S. A.* **2011**, *108*, 937−943.
(23) Hayek, K.; Kramer, R.; Paál, Z. *Appl. Catal., A* **1997**, *162*, 1−15.
(24) Green, I. X.; Tang, W.; Neurock, M.; Yates, J. T., Jr.; J. T., Y. *Science (80-.)* **2011**, *333*, 736−739.
(25) Green, I. X.; Tang, W.; Neurock, M.; Yates, J. T. *Faraday Discuss.* **2013**, *162*, 247.
(26) Kaden, W. E.; Kunkel, W. a.; Roberts, F. S.; Kane, M.; Anderson, S. L. *J. Chem. Phys.* **2012**, *136*, 204705.
(27) Kaden, W. E.; Kunkel, W. a.; Kane, M. D.; Roberts, F. S.; Anderson, S. L. *J. Am. Chem. Soc.* **2010**, *132*, 13097−9.
(28) Fischer, F.; Tropsch, H. *Brennstoff-Chem.* **1926**, *7*, 97.
(29) Fischer, F.; Tropsch, H. *Brennstoff-Chem.* **1930**, *11*, 489.
(30) Mei, D.; Rousseau, R.; Kathmann, S. M.; Glezakou, V.-A.; Engelhard, M. H.; Jiang, W.; Wang, C.; Gerber, M. A.; White, J. F.; Stevens, D. J. *J. Catal.* **2010**, *271*, 325−342.
(31) Chuang, S. S. C.; Stevens, R. W.; Khatri, R. *Top. Catal.* **2005**, *32*, 225−232.
(32) Liu, Y.; Murata, K.; Inaba, M.; Takahara, I.; Okabe, K. *Catal. Today* **2011**, *164*, 308−314.
(33) Gogate, M. R.; Davis, R. J. *ChemCatChem* **2009**, *1*, 295−303.
(34) Dalai, A.; Davis, B. *Appl. Catal., A* **2008**, *348*, 1−15.
(35) Yan, Z.; Bukur, D. B.; Goodman, D. W. *Catal. Today* **2011**, *160*, 39−43.
(36) Wang, J.; Zhang, Q.; Wang, Y. *Catal. Today* **2011**, *171*, 257−265.
(37) Li, P.; Liu, J.; Nag, N.; Crozier, P. *Surf. Sci.* **2006**, *600*, 693−702.
(38) Stakheev, A.; Kustov, L. *Appl. Catal., A* **1999**, *188*, 3−35.
(39) Diebold, U. *Surf. Sci. Rep.* **2003**, *48*, 53−229.
(40) Perron, H.; Domain, C.; Roques, J.; Drot, R.; Simoni, E.; Catalette, H. *Theor. Chem. Acc.* **2007**, *117*, 565−574.
(41) Morgan, B. J.; Watson, G. W. *Surf. Sci.* **2007**, *601*, 5034−5041.
(42) Kunat, M.; Burghaus, U.; Wöll, C. *Phys. Chem. Chem. Phys.* **2004**, *6*, 4203.
(43) Menetrey, M.; Markovits, a.; Minot, C. *Surf. Sci.* **2003**, *524*, 49−62.
(44) Suda, Y.; Morimoto, T. *Langmuir* **1987**, *3*, 786−788.
(45) Prins, R. *Chem. Rev.* **2012**, *112*, 2714−2738.
(46) Murashov, V. V.; Demchuk, E. *Surf. Sci.* **2005**, *595*, 6−19.
(47) Goumans, T. P. M.; Wander, A.; Brown, W. A.; Catlow, C. R. A. *Phys. Chem. Chem. Phys.* **2007**, *9*, 2146−2152.
(48) Rignanese, G.-M.; De Vita, A.; Charlier, J.-C.; Gonze, X.; Car, R. *Phys. Rev. B* **2000**, *61*, 13250−13255.
(49) Sneh, O.; George, S. M. *J. Phys. Chem.* **1995**, *99*, 4639−4647.
(50) Michalske, T. A.; Freiman, S. W. *Nature* **1982**, *295*, 511−512.
(51) Beyer, H.; Emmerich, J.; Chatziapostolou, K.; Köhler, K. *Appl. Catal., A* **2011**, *391*, 411−416.
(52) Ligthart, D.; van Santen, R.; Hensen, E. *J. Catal.* **2011**, *280*, 206−220.
(53) Wang, Z.-j.; Yang, F.; Axnanda, S.; Liu, C.-j.; Goodman, D. W. *Appl. Catal., A* **2011**, *391*, 342−349.
(54) Gao, J.; Mo, X.; Chien, A. C.-Y.; Torres, W.; Goodwin, J. G., Jr. *J. Catal.* **2009**, *262*, 119−126.
(55) Mo, X.; Gao, J.; Goodwin, J. G., Jr. *Catal. Today* **2009**, *147*, 139−149.
(56) Mo, X.; Gao, J.; Umnajkaseam, N.; Goodwin, J. G., Jr. *J. Catal.* **2009**, *267*, 167−176.
(57) Savastenko, N.; Volpp, H.-R.; Gerlach, O.; Strehlau, W. *J. Nanoparticle Res.* **2008**, *10*, 277−287.
(58) Ito, S.-i.; Chibana, C.; Nagashima, K.; Kameoka, S.; Tomishige, K.; Kunimori, K. *Appl. Catal., A* **2002**, *236*, 113−120.
(59) Barthe, L.; Hemati, M.; Philippot, K.; Chaudret, B.; Denicourt-nowicki, A.; Roucoux, A. *Chem. Eng. J.* **2009**, *151*, 372−379.
(60) Somorjai, G. A.; Aliaga, C. *Langmuir* **2010**, *26*, 16190−16203.
(61) van Santen, R. A.; Neurock, M.; Shetty, S. G. *Chem. Rev.* **2010**, *110*, 2005−2048.
(62) Van Santen, R. A. *Acc. Chem. Res.* **2008**, *42*, 57−66.
(63) Schwartz, V.; Campos, A.; Egbebi, A.; Spivey, J. J.; Overbury, S. H. *ACS Catal.* **2011**, *1*, 1298−1306.
(64) Beale, A. M.; Weckhuysen, B. M. *Phys. Chem. Chem. Phys.* **2010**, *12*, 5562−5574.
(65) Logan, A. D.; Braunschweig, E. J.; Datye, A. K.; Smith, D. J. *Langmuir* **1988**, *4*, 827−830.
(66) Liu, Z.-P.; Hu, P. *J. Am. Chem. Soc.* **2001**, *123*, 12596−12604.
(67) Filot, I. A. W.; Shetty, S. G.; Hensen, E. J. M.; van Santen, R. A. *J. Phys. Chem. C* **2011**, *115*, 14204−14212.
(68) Liu, Z.-P.; Hu, P. *J. Chem. Phys.* **2001**, *114*, 8244.
(69) Mavrikakis, M.; Bäumer, M.; Freund, H.-J.; Nørskov, J. K. *Catal. Lett.* **2002**, *81*, 153−156.
(70) Zhang, R.; Sun, X.; Wang, B. *J. Phys. Chem. C* **2013**, *117*, 6594−6606.
(71) Kapur, N.; Hyun, J.; Shan, B.; Nicholas, J. B.; Cho, K. *J. Phys. Chem. C* **2010**, *114*, 10171−10182.
(72) Subramanian, N. D.; Gao, J.; Mo, X.; Goodwin, J. G., Jr.; Torres, W.; Spivey, J. J. *J. Catal.* **2010**, *272*, 204−209.
(73) Choi, Y.; Liu, P. *J. Am. Chem. Soc.* **2009**, *131*, 13054−13061.
(74) Bahn, S. R.; Jacobsen, K. W. *Comput. Sci. Eng.* **2002**, *4*, 56−66.

(75) Kresse, G.; Hafner, J. *Phys. Rev. B* **1993**, *47*, 558−561.
(76) Kresse, G.; Hafner, J. *Phys. Rev. B* **1994**, *49*, 14251−14269.
(77) Kresse, G.; Furthmüller, J. *Comput. Mater. Sci.* **1996**, *6*, 15.
(78) Kresse, G.; Furthmüller, J. *Phys. Rev. B* **1996**, *54*, 11169−11186.
(79) Perdew, J. P.; Burke, K.; Ernzerhof, M. *Phys. Rev. Lett.* **1996**, *77*, 3865−3868.
(80) Blöchl, P. E. *Phys. Rev. B* **1994**, *50*, 17953−17979.
(81) Kresse, G. *Phys. Rev. B* **1999**, *59*, 1758−1775.
(82) Davidson, E. R. In *Methods in Computational Molecular Physics*; Diercksen, G. H. F., Wilson, S., Eds.; NATO Advanced Study Institute, Series C; Springer: New York, 1983; Vol. *113*, p 95.
(83) Pulay, P. *Chem. Phys. Lett.* **1980**, *73*, 393−398.
(84) Wood, D. M.; Zunger, A. *J. Phys. A: Math. Gen.* **1985**, *18*, 1343−1359.
(85) Monkhorst, H. J.; Pack, J. D. *Phys. Rev. B* **1976**, *13*, 5188−5192.
(86) Dudarev, S. L.; Savrasov, S. Y.; Humphreys, C. J.; Sutton, A. P. *Phys. Rev. B* **1998**, *57*, 1505−1509.
(87) Hu, Z.; Metiu, H. *J. Phys. Chem. C* **2011**, *115*, 5841−5845.
(88) Bitzek, E.; Koskinen, P.; Gähler, F.; Moseler, M.; Gumbsch, P. *Phys. Rev. Lett.* **2006**, *97*, 1−4.
(89) Hammer, B.; Nørskov, J. K. *Surf. Sci.* **1995**, *343*, 211−220.
(90) Li, L.; Larsen, A. H.; Romero, N. a.; Morozov, V. a.; Glinsvad, C.; Abild-Pedersen, F.; Greeley, J.; Jacobsen, K. W.; Nørskov, J. K. *J. Phys. Chem. Lett.* **2013**, *4*, 222−226.
(91) Rapps, T.; Ahlrichs, R.; Waldt, E.; Kappes, M. M.; Schooss, D. *Angew. Chem., Int. Ed.* **2013**, 6102−6105.
(92) Shustorovich, E. *Adv. Catal.* **1990**, *37*, 101.
(93) Tang, W.; Sanville, E.; Henkelman, G. *J. Phys.: Condens. Matter* **2009**, *21*, 084204.
(94) Sanville, E.; Kenny, S. D.; Smith, R.; Henkelman, G. *J. Comput. Chem.* **2007**, *28*, 899−908.
(95) Hughbanks, T.; Hoffmann, R. *J. Am. Chem. Soc.* **1983**, *105*, 3528−3537.
(96) Grechnev, A.; Ahuja, R.; Eriksson, O. *J. Phys.: Condens. Matter* **2003**, *15*, 7751−7761.
(97) Sanchez-Portal, D.; Artacho, E.; Soler, J. M. *Solid State Commun.* **1995**, *95*, 685−690.
(98) Sánchez-Portal, D.; Artacho, E.; Soler, J. M. *J. Phys.: Condens. Matter* **1996**, *8*, 3859−3880.
(99) Dunnington, B. D.; Schmidt, J. R. *J. Chem. Theory Comput.* **2012**, *8*, 1902−1911.
(100) Bronsted, J. N. *Chem. Rev.* **1928**, *5*, 231−338.
(101) Evans, M. G.; Polanyi, M. *Trans. Faraday Soc.* **1938**, *34*, 11.
(102) Michaelides, A.; Liu, Z.-P.; Zhang, C. J.; Alavi, A.; King, D. a.; Hu, P. *J. Am. Chem. Soc.* **2003**, *125*, 3704−3705.
(103) Nørskov, J.; Bligaard, T.; Logadottir, A.; Bahn, S. R.; Hansen, L. B.; Bollinger, M.; Bengaard, H.; Hammer, B.; Sljivancanin, Z.; Mavrikakis, M.; Xu, Y.; Dahl, S.; Jacobsen, C. J. H. *J. Catal.* **2002**, *209*, 275−278.
(104) Wang, S.; Petzold, V.; Tripkovic, V.; Kleis, J.; Howalt, J. G.; Skulason, E.; Fernandez, E. M.; Hvolbaek, B.; Jones, G.; Toftelund, A.; Falsig, H.; Bjorketun, M.; Studt, F.; Abild-Pedersen, F.; Rossmeisl, J.; Nørskov, J. K.; Bligaard, T. *Phys. Chem. Chem. Phys.* **2011**, *13*, 20760−20765.
(105) Gao, J.; Mo, X.; Goodwin, J. G., Jr. *J. Catal.* **2009**, *268*, 142−149.
(106) Haider, M. A.; Gogate, M. R.; Davis, R. J. *J. Catal.* **2009**, *261*, 9−16.
(107) Egbebi, A.; Schwartz, V.; Overbury, S. H.; Spivey, J. J. *Catal. Today* **2010**, *149*, 91−97.
(108) Gogate, M. R.; Davis, R. J. *Catal. Commun.* **2010**, *11*, 901−906.
(109) Loveless, B. T.; Buda, C.; Neurock, M.; Iglesia, E. *J. Am. Chem. Soc.* **2013**, *135*, 6107−6121.
(110) Allian, A. D.; Takanabe, K.; Fujdala, K. L.; Hao, X.; Truex, T. J.; Cai, J.; Buda, C.; Neurock, M.; Iglesia, E. *J. Am. Chem. Soc.* **2011**, *133*, 4498−4517.
(111) Kose, R.; Brown, W. a.; King, D. a. *J. Phys. Chem. B* **1999**, *103*, 8722−8725.
(112) van Bavel, a. P.; Hopstaken, M. J. P.; Curulla, D.; Niemantsverdriet, J. W.; Lukkien, J. J.; Hilbers, P. a. J. *J. Chem. Phys.* **2003**, *119*, 524.
(113) Mars, P.; van Krevelen, D. *Chem. Eng. Sci.* **1954**, *3*, 41−59.
(114) Kim, H. Y.; Park, J.-N.; Henkelman, G.; Kim, J. M. *ChemSusChem* **2012**, *0165*, 1474−1481.
(115) Park, J.; Renzas, J.; Hsu, B.; Somorjai, G. *J. Phys. Chem. C* **2007**, *111*, 15331−15336.
(116) Somorjai, G.; Park, J. *Top. Catal.* **2008**, *49*, 126−135.